3D micro printed internally wetted capillary type electrospray emitters on the single micrometer scale

IEPC-2022-175

Presented at the 37th International Electric Propulsion Conference
Massachusetts Institute of Technology, Cambridge, MA, USA
June 19-23, 2022

Fynn Kunze[1], Jana Zorn[2], Torsten Henning[3], Kristof Holste[4] and Peter J. Klar [5]
Justus-Liebig-University Giessen, Heinrich-Buff-Ring 16, 35392 Giessen, Germany

Internally wetted capillary type electrospray emitters arrays fabricated by 3D micro printing are presented. The emitter arrays consist of more than 200 individual emitters in different configurations. Fabricated from pure SU-8 photo epoxy the emitters show very high mechanical, chemical and radiation resistances. Furthermore, a time of flight set-up for the characterization of the emission from such emitter arrays is presented and preliminary time of flight data is shown.

I. Nomenclature

EMIM-BF_4	=	1-Ethyl-3-methylimidazolium tetrafluoroborate (an ionic liquid)
E_{el}	=	Electric energy
E_{kin}	=	Kinetic energy
g_0	=	Gravitational constant of the earth
I_{sp}	=	Specific impulse
L	=	Flight path length
m	=	Ion mass
q_{sp}	=	Ion charge
T_{flight}	=	Particle flight time
U_{extr}	=	Extraction voltage
v_{ion}	=	Ion velocity

II. Motivation and introduction

The ESA prognoses the number of small space craft already and to be launched to increase exponentially by the year. Already more than 1000 satellites will be launched by 2022 and up to 50 000 small spacecraft will be in orbit by 2030 [1]. Driving factor for the commercial interest are massive constellations such as Starlink and OneWeb as well as the more easily accessible rides. Highly integrated thruster systems with as small as possible mass and lateral dimensions for the application on small, micro and nano satellites are in high demand, Furthermore, with the already sparse Xenon supplies, plasma based thrusters may not be the optimal choice in the future, which leads to the development of new innovative thruster solutions. Electrospray emitters are an interesting choice as a micropropulsion solution. They offer a very high specific impulse, low power requirements and precise thrust management, which makes them a very good choice for micro and nano satellites [2–4]. Furthermore, they are highly miniaturizable and even scale favorably on

[1]PhD cand., Institute of Experimental Physics I and Center for Materials Research, Fynn.Kunze@physik.jlug.de
[2]MSc cand., Institute of Experimental Physics I, Jana.Zorn@physik.jlug.de
[3]Senior staff scientist, Institute of Experimental Physics I and Center for Materials Research, Torsten.Henning@physik.jlug.de
[4]Senior staff scientist, Institute of Experimental Physics I, Kristof.Holste@physik.jlug.de
[5]Director of Institute of Experimental Physics I and Center for Materials Research, Head of EP-group, Peter.J.Klar@exp1.physik.uni-giessen.de

miniaturization. Additionally they may be operated with liquid metal or ionic liquids, two readily available propellants. Liquid metal based thrusters from e.g Enpulsion have flight heritage [5] and are currently in high demand with over 100 units of the EnpulsionNano sold in 2022 [6]. This indicates a high interest in electrospray propulsion systems and the need to develop novel electrospray systems, such as the micro 3D printed emitters presented here.

Electrospray emitters operate by applying a static electrical voltage between an extraction electrode and a liquid propellant. Most commonly used are liquid metals or ionic liquids, which are easy to ionize or are already ionized. The propellant exposed to the electrical field forms a conic shape towards the extraction electrode, a so called Taylor cone [7]. The electrical field at the tip of the cone is amplified to a degree where the propellant is ionized and already existing ions are able to leave the propellant forming a spray of ions or droplets. Electrospray emitters can operate in different spray modes, each having its own characteristics. For example, droplet spray mode extracts mass rich heavy droplets at comparably low velocities, while ion spray mode extracts single ions at high speed [8]. Currently there are three dominant emitter types used. Porous emitter types supply the propellant through their porous structure to the surface where it can interact with the electrical field [8]. An example are the emitters manufactured by Enpulsion which use a tungsten sponge as base material to form conic emitter structures. These emitters rely on the the statistical distribution of the pores to evenly supply the propellant to the surface an thus are limited regarding their size and shape by the characteristics of the porous material. There are approaches to manufacture uniform porous materials by sintering silica pearls, however, this is part of ongoing research [9]. The second emitter type is the externally wetted emitter type [8]. These emitters supply the propellant over the surface of an emission structure, like a cone or an edge. The challenge of this emitter type is to get the right amount of propellant onto the surface. If to much liquid is supplied, unwanted interaction may occur and impede or influence the formation of an controlled ion spray. Last type of emitter are internally wetted capillary type emitters [8, 10, 11]. For this kind of emitter the propellant is fed through thin capillaries and is extracted from the orifice at the end of the capillary. Challenging for this type of emitter is the low hydraulic resistance, which may easily lead to propellant spilling out of the capillary and wet the structures around the orifice, thus impeding intended operation [12]. A way to approach this challenge is the application of a 3D micro printing technology, the two photon lithography. This manufacturing method allows the additive manufacturing of high aspect ratio capillaries with a high degree of freedom The freedom of design also includes the fluid paths where flow inhibiting structures may be included. Thus the hydraulic resistance can be tailored to the specific application intended for the emitters. This is also our approach to a novel electrospray design, which uses a photo sensitive polymer, called SU-8, as base material and is fabricated by two photon lithography.

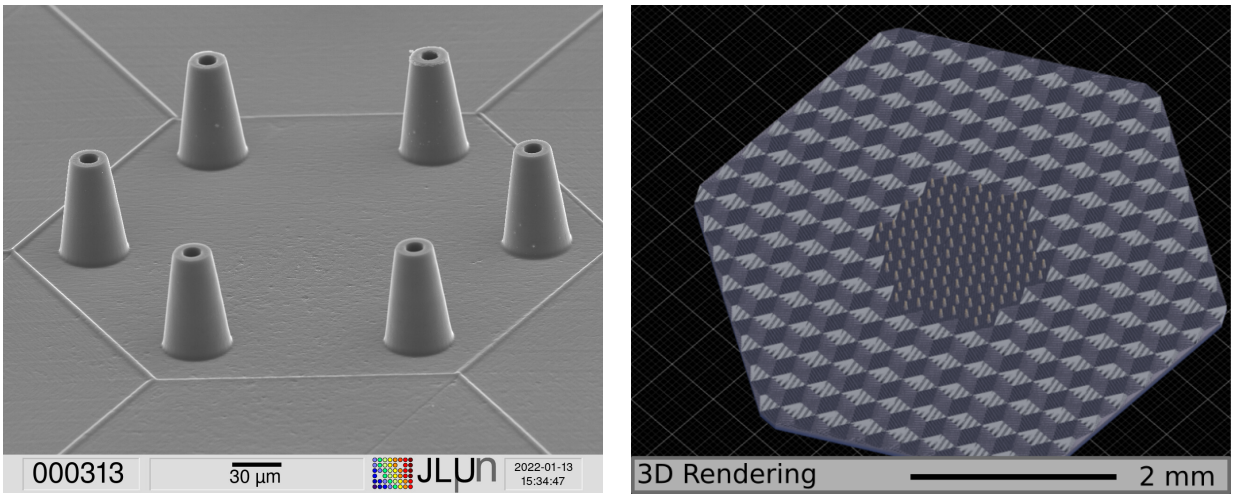

(a) **(b)**

Fig. 1 (a) SEM image of a 3D printed cluster of six individual emitters and (b) a 3D rendering of an advanced emitter array with more than 200 individual emitters

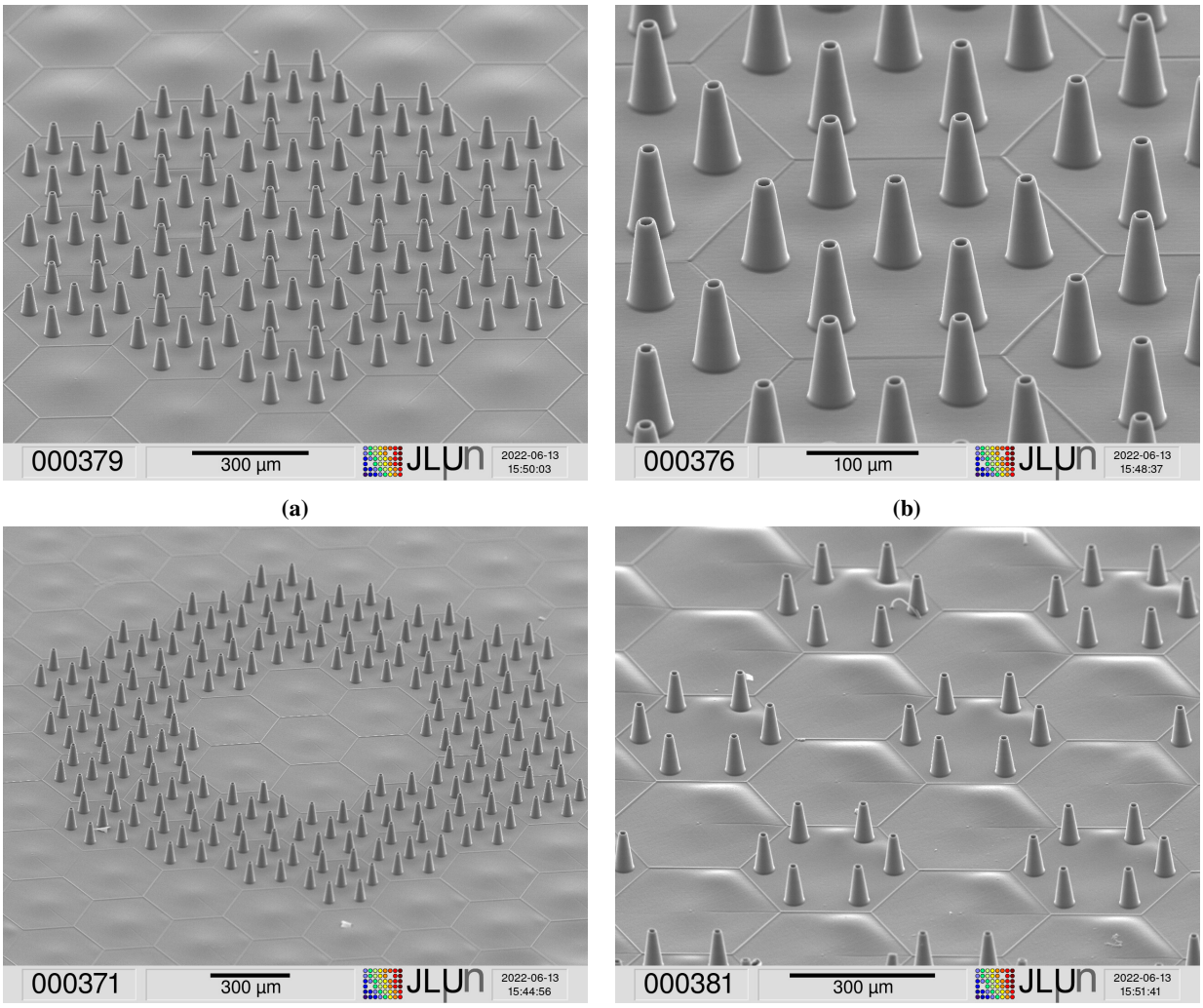

Fig. 2 SEM images of multiple array configurations with (a) the emitter array from Fig. 1b with more than 200 emitters evenly distributed emitters, (b) a close up shot of the same array, (c) an array in ring configuration and (d) an array in cluster configuration.

III. Manufacturing of emitters and arrays

The feasibility of the manufacturing of electrospray emitters by photo lithography has already been proven by the authors. Emitter and even some arrays have been manufactured by 2D planar [13–15] and 3D lithography (two photon lithography) [10, 11]. A process to reliably micro 3D print capillary type electrospray emitters with capillary diameters in the singe micrometer range has been reported by the authors in 2021 [10]. The core of this manufacturing method is the application of the two photon lithography. Two photon lithography uses a near infrared pulsed laser, which is focused through a microscope objective into a layer of photoresist. The photons emitted by the laser have on their own too little energy to trigger a photo chemical reaction in a typical photo sensitive resin, in our case SU-8. Only at the focal point of the laser the intensity is sufficiently high to trigger two photon absorption processes at a very high rate, while the unfocused part of the laser beam just passes through the photoresist. While one photon carries to little energy, two photons, however, provide a similar energy as an ultra violet photon, thus triggering the photo reaction in the resin. By scanning the focal point through the resin in all three dimensions, any 3D structure can be written to the resin layer. If used with an negative tone photoresist, like SU-8, the exposed areas harden and can be washed out of the unexposed resin after the process. The exact process parameters were reported by the author in 2021 [10]. SU-8 is

already validated as a suitable material for space applications. It shows high mechanical and chemicals stability and is very resistant to electromagnetic and particle radiation [11, 16]. A resulting emitter cluster with six emitters is shown in Fig. 1a as well as a selection of arrays are shown in Fig. 2.

The 3D lithography further allows the fabrication of advanced emitter arrays. As the individual emitters are very small and only provide a fraction of a nanonewton of thrust, usable thrust levels can be achieved by increasing the number of emitters. The authors have proven, the reliability and print quality over a large printing area [10, 11]. This allows the fabrication of emitter arrays consisting of hundreds of individual emitters. Furthermore, due to the high freedom of design the emitter arrays can also be tailored according to the user's wishes. The individual emitter shape, structure and position in the array can be chosen freely. Figure 1b shows a render of an evenly distributed emitter array and Fig. 2a shows a SEM image of the finished array. The individual emitters are identical in form and spaced equidistant, thus representing one of the simpler array configurations. A close up shot shown in Fig. 2b of the center part of the array shows the high reprinting precision and overall print quality. It is possible to use the same program code, which resulted in the even distribution array in Fig. 1b to fabricate ring arrays or arrays of smaller grouped clusters, which are shown in Fig. 2c and Fig. 2d. These arrays are more complex and show the advantages of this fabrication method. All of the presented arrays were fabricated in the same batch process using the same printing program, with a printing time of less than 7 h per whole emitter array, including the emitters as well as a supporting base around them. One complete emitter array measures about 5 mm in diagonal, with the active emitter area as small as 1 mm to 1.5 mm in diameter.

IV. Time of flight experiments

Time of flight experiments (ToF) are a necessary step to determine the performance and the extraction behavior of electrospray thrusters. Depending on the type of extraction mode emitters can output ions, droplets, or a mixture of both in varying ratios. Depending on the spray mode, either more thrust by extracting heavy droplets or higher specific impulse I_{sp} by extracting pure ions can be achieved. Time of flight experiments give insight into plume composition, ion velocity and mass distribution at a given point of operation of the emitter array.

The concept of time of flight measurements stems initially from nuclear physics, which focuses on single particles or atoms and the occurring reactions at high energies. At its core ToF relies on the law of energy conservation to gain information about the kinetic energy E_{kin} of a given particle by sending it along a predetermined path of a certain length L and measuring the time it needs to travel one way. The flight time T_{flight} in conjunction with the path length L gives information about the velocity v_{ion} of the particle.

$$v_{ion} = \frac{L}{T_{flight}} \tag{1}$$

If either the mass m or the starting energy E_{start} of the particle is known, one can calculate the missing information from Eq. (2).

$$E_{kin} = \frac{1}{2} m v_{ion}^2 = E_{start} \tag{2}$$

For our purpose of extraction from electrospray emitters, the energy at which the particles start is given by the extraction voltage U_{extr} and the charge of the particle q, thus can be described by Eq. (3).

$$E_{start} = E_{el} = qU_{extr} \tag{3}$$

By combining Eq. (1), Eq. (2) and Eq. (3) we can calculate the mass m of a detected particle for a fixed set-up with a path length L.

$$m = \frac{2qU}{v_{ion}^2} = 2qU_{extr}\frac{T_{flight}^2}{L^2} \tag{4}$$

Furthermore, the specific impulse I_{sp} can also be calculated from Eq. (1) by dividing the velocity v_{ion} by the gravitational constant of the earth g_0.

$$I_{sp} = \frac{v_{ion}}{g_0} = \frac{L}{g_0 T_{flight}} \tag{5}$$

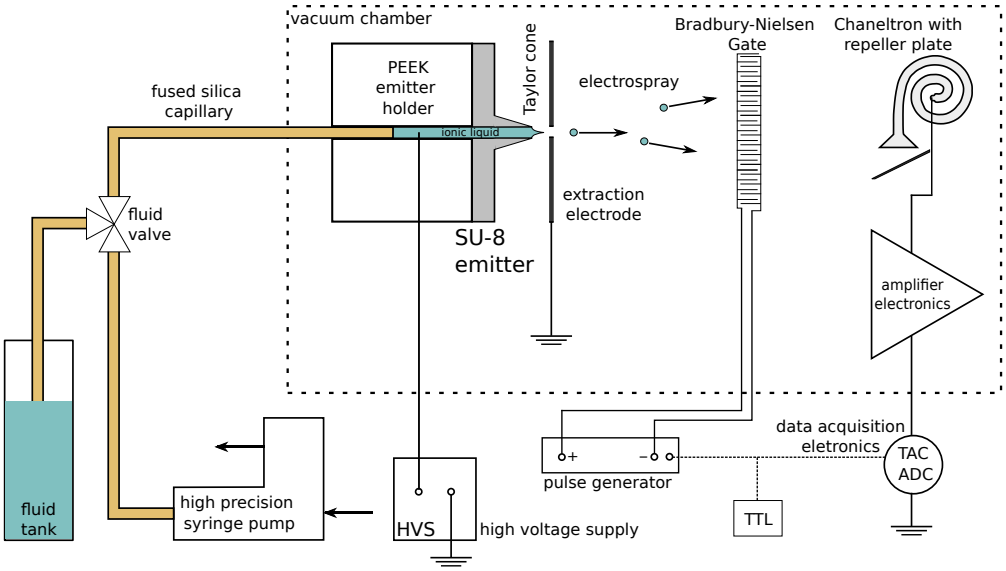

Fig. 3 Schematic drawing of the set-up for the time of flight experiments.

A. Experimental set-up

For the time of flight experiments we use the previously reported experimental set-up for the characterization of electrospray emitters at the JLU [10, 11]. Additionally to the set-up already in use, a Bradbury-Nielsen ion gate was integrated into the flight path to control the ion beam. Furthermore, the collector plate from the previous DC characterization set-up was exchanged for a channeltron detector with a much higher detection sensitivity. A schematic drawing of the set-up is shown in Fig. 3.

To acquire time of flight data from ion sources operating at constant or semi constant emission mode, the ion beam has to be chopped into small packages which do not overlap, meaning one whole package can reach the detector before next package is sent on its way. If the time frame of a single package is to o long, very fast ions from the next package can interfere with measurement of the previous package. Is the time frame too short few ions can pass the gate and result in very low detection rates and thus long measurement times. Therefore, an ion gate is necessary to reliably control the ion intake to the detector. We opt for an Bradbury-Nielsen gate, which will be discussed in more detail below. The gate is controlled by two independent DEI PVX-4130 ±6kV pulse generators. One is connected to an controllable positive HV source, the second is connected to a negative HV source. Both pulse generators are gated by a 5V square-wave transistor-transistor-logic (TTL) signal provided by a ROHDE & SCHWARZ HM8150 programmable function generator. Due to an electrical restriction of the pulse generators, which allows one only to switch from a lower potential to a higher potential, the pulse generator connected to the positive HV source has to be controlled by an inverted TTL signal. We use a single inverter gate to invert the TTL signal provided by the function generator. The data signal obtained from the channeltron is fed into an ORTEC VT120 fast preamplifier and afterwards passed through a ROENTDEK CFD1x constant fraction discriminator to eliminate time delays due to different pulse heights. Both the TTL signal and the signals from the CFD are fed into a CANBERRA MODEL 2043 time analyzer, with the TTL signal connected to the start input and the CFD signal to the stop input. The time analyzer translates the time delay between start and stop into a voltage signal ranging from 0 to 10 V, sorted from short to long. This 0 to 10 V signal is output from the time analyzer via the time to amplitude converted (TAC) output, which connects to an analog to digital converter ADC/ND-560 from NUCLEAR DATA . The ADC converters the TAC signal into 1024 or 2048 channels, depending on the device settings, and send these to an external computer to save the data. The fight time T_{flight} can be calculated using Eq. (6) from the time analyzer range T_{max}, the channel number C_{i} and the maximum number of channels C_{max}.

$$T_{\text{flight}} = \frac{T_{\text{max}}}{C_{\text{max}}} C_{\text{i}} \tag{6}$$

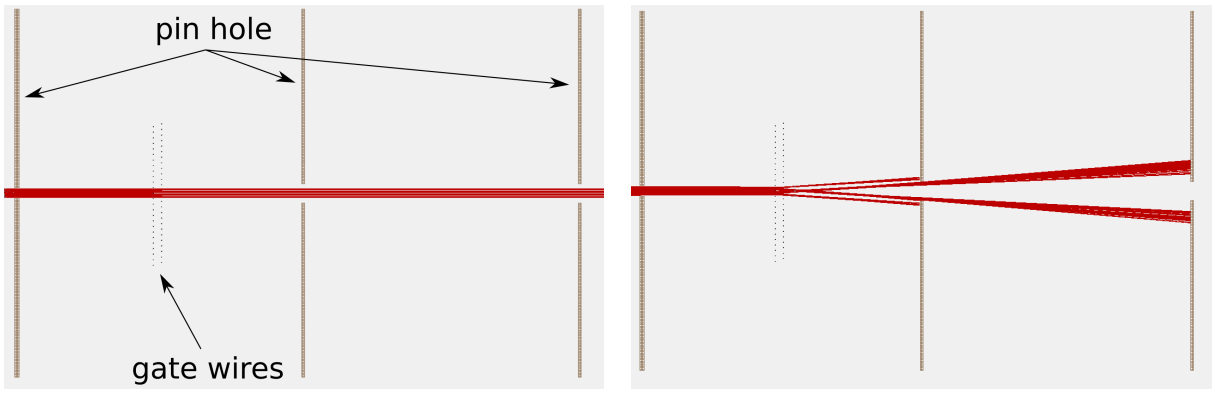

(a) (b)

Fig. 4 SIMION simulation of the flight path of ions through a Bradbury-Nielsen gate in (a) the open state and in (b) the closed state

B. Bradbury-Nielsen-Gate

In mass spectroscopy experiments ion gates are commonly used to deflect and steer ion beams. The gate is necessary in flight time experiments to control when ions may pass through to the detector. A widely used ion gate is the Bradbury-Nielsen ion gate [17]. Due to its comparably easy structure, fast reaction times and high precision, Bradbury-Nielsen gates are a logical choice for such experiments. The gate consists of two isolated wire grids placed in the same plane. The wires are alternated in such a way that neighboring wires are not connected, but the second neighbors are. The wires are commonly wound up on an external structure similar to guitar strings or are etched out very thin metal sheets. To operate the ion gate, one set of wires is placed at a negative potential while the other set is placed at an positive potential. This leads to local strong fields between the wires. However, if the potentials are applied symmetrically no far field is generated. If an ion comes near the wires while the voltages are applied to the wires the electrical attraction and repulsion from the positive and negative wires deflect the ion, independent of the type of charge, outwards. Therefore, no ions could pass the plane the wires are positioned without getting deflected. If coupled with a set of pinholes, no ions may reach the detector of the set-up while the voltage is applied [17]. This translates to a closed gate state. To open the gate one has to simply stop applying a voltage to the wires. The open close cycle, thus is only dependent on the speed at which the voltage can be applied. With the right electronics the switch between opened and closed state of the gate can be achieved in few a nanoseconds.

We opt to build our own Bradbury-Nielsen gate and therefore started with a simulation of the flight path of the expected ions in SIMION, a simulation software commonly used in nuclear physics to simulate ion flight paths, to compare different gate configurations. The simulation uses the ion masses of EMIM-BF_4, an ionic liquid commonly used in electrospray applications with the compound masses of 86.8 u for the anion BF_4^- and 111.37 u for the cation $EMIM^+$ as well as a kinetic energy of 4 keV for both ion species. The gate is simulated using a wire diameter of 0.2 mm, a wire distance of 0.6 mm and two pinholes at a distance of 30 mm in front and behind the gate with a through hole diameter of 4 mm. As gate voltages ±500 V were applied to the wires. The results from the simulation of 1000 ions are shown in Fig. 4, with a open gate in Fig. 4a and a closed gate in Fig. 4b. We further simulated a complete open-close cycle of the whole gate driven by a square wave voltage signal simulated using the Gibbs phenomenon from 0 to ±500 V and calculated transmission coefficient from the results. The results show no transmission for the EMIM-BF_4 ions if the gate in closed and a transmission of approximately 72 % for an open gate. The 30 % loss can be explained by the collision of ions with the wires while the gate is open. Nevertheless, these results are very promising for the ion gate, as a low ion rate can be beneficial for the detection, especial for very sensitive detectors, where one can compensate for a low rate by prolonging the measurement time.

We manufactured the gate according to the parameters used for the simulation. A 3D CAD drawing of the gate alongside a picture of the finished product is shown in Fig. 5. We decided to go with a single tension wire instead of an etched wire mesh as manufacturing and necessary repairs are more facile. The gate consist of two individual wire holders, with each holding one wire mesh. In Fig. 5b both holders are screwed together to from the complete gate. A spring steel wire with a diameter of 0.2 mm is wound around small steel pins embedded in a PEEK holder on one side

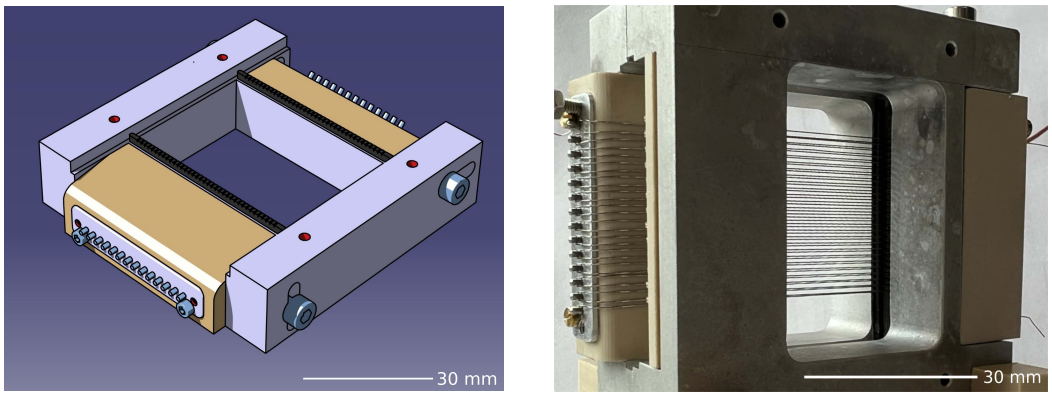

(a) **(b)**

Fig. 5 (a) CAD rendering of one half of the Bradbury-Nielsen gate alongside (b) a picture of the finish product

and an steel holder inserted in a PEEK casing on the other side. The two screws at the top and bottom of the steel holder visible in the picture define the attachment points for the wire. It is possible to control the tension of the wire by two grub screws which can move the whole steel holder outward. To guarantee a perfect spacing the wire is run trough a plastic spacer with conic grooves cut into at fixed distances of 1.2 mm. With both wire holders screwed together at an small offset, a wire mesh with a wire distance of 0.6 mm is generated. Both wire spools are completely electrically insulated from each other as no physical contact is possible. The small offset between both wire sets perpendicular to the plane due to the distance between both holders is negligible and does not impact the operation of the gate. We integrated the gate into the set-up described in Fig. 3 tested its performance. The gate performed as expected with no transmission while closed and high transmission while opened.

V. Preliminary ToF results

We started preliminary time of flight measurements with EMIM-BF_4 as an ion source extracted from a steel capillary at different extraction voltages. For the experiments we used the set-up described in Sec. IV with the aforementioned Bradbury-Nielsen gate and operated the set-up under the condition listed in Table 1.

We obtained the flight time data for EMIM-BF_4 shown in Fig. 6. Two spectra are shown from two independent measurements, with different settings for the time analyzer. The flight time was derived from the raw data obtained from the ADC following Eq.(6) and thus is only based on the assumption about the conditions listed in Table 1. further validation is required. This preliminary estimation will not result in the true flight time data, as we cannot exclude any unwanted interactions of the ions, but it should suffice to estimate the range of the flight time and mass of the detected ions. For measurements shown in Fig. 6a a time range of 20 µs was selected for the device. To get a closer look at the

Table 1 Experimental conditions for ToF experiment

Propellant	EMIM-BF_4
Emitter	Steel capillary ∅ 100 µm
Electrode	Copper ring ∅ 5 mm
Electrode distance	6 mm
Extraction voltage	-5 kV
Feed rate	0.1 µl/min
Gate voltage	±1000 V
Gate open time	1 µs
Gate switching frequency	100 Hz
Flight path length	0.8 m
Time analyzer range	20 µs and 10 µs
ADC channels	2048

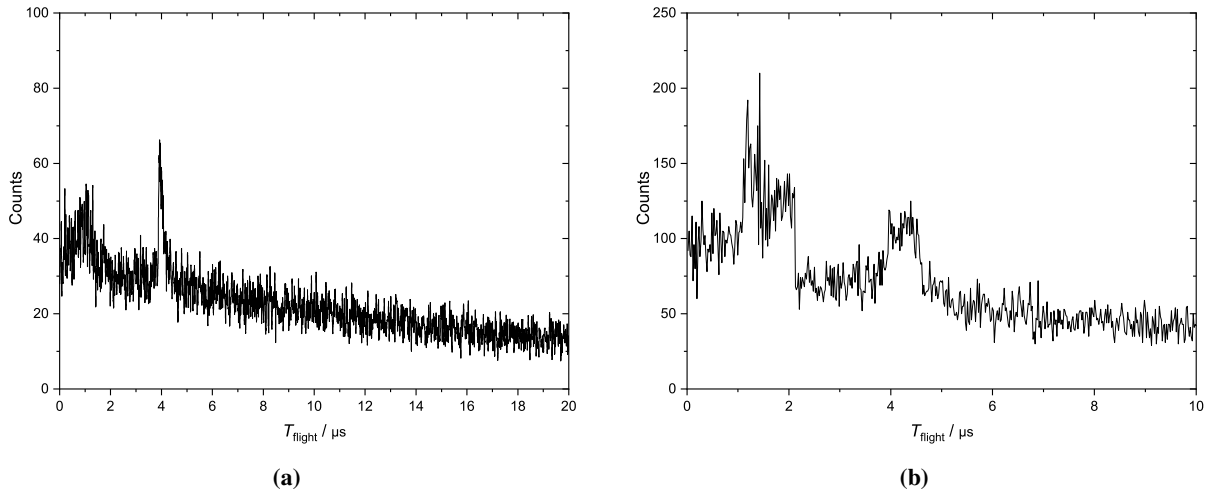

Fig. 6 Results from the preliminary time of flight measurements with the assumed (a) flight time and a time range of 20 µs and (b) a second flight time spectrum with a time range of 10 µs at 5 kV extraction voltage and EMIM-BF_4 as source

local maxima in the left part of the spectrum we repeated the measurements a second time, with a time range of 10 µs. The corresponding results are shown in Fig. 6b.

Both spectra show similar local maxima at the same flight times, at 1.2 µs, 1.8 µs and 4.5 µs. The reproducibility indicates that the data obtained truly show ions and not some electrical noise. Furthermore, no signal occurs when a physical valve in the beam path is closed, thus physically separating the source from the detector. A similar effect on the signal is achieved by permanently closing the Bradbury-Nielsen gate. No ions may reach the detector if the gate voltages are applied constantly. We also observed the difference in signal with a pulsed gate and a permanently open gate. For a permanently open gate the signal is constant over the whole time range, while a pulsed gate results in the signal shown above. The spectrum shown in Fig. 6a exhibits a small exponential decay, witch can be accounted to not optimized electronic settings and the set-up itself. The holder of the pins holes used to collect the ions deflected by the Bradbury-Nielsen gate are maybe too small and some defected ions may still pass around them, thus leading to free ions in the vacuum chamber with a exponential velocity distribution. For the more focused spectrum in Fig. 6b this effect is a lot less dominant due to the smaller time frame. The distribution is closer to a linear offset and has overall less impact on the results. These assumed flight times translate with a path length of 0.8 m to a I_{sp} range from $6.7 \cdot 10^4$ s for the 1.2 µs flight time to $1.78 \cdot 10^4$ s for the flight time of 4.5 µs.

We also estimate the mass from the flight times by applying Eq. (4) under the same assumptions as before. For a more precise interpretation of the obtained data we need to calibrate the device beforehand with a known spectrum, from which we can reference the data. The assumed masses of the ions responsible for the local maxima observable in the spectra are approximately 2 u for the 1.2 µs fight time, 6 u for the 1.8 µs flight time and 23 u to 31 u for the broad maximum at 4.5 µs flight time. Like stated before, the spectrum is not calibrated and therefore, could display the maxima at the wrong position. In the current uncalibrated state we can olay make an educated guess which peak correlats to whihc ion. As EMIM-BF_4 is used with a negative voltage applied to the ionic liquid BF_4^- are expected to be extracted, but the mass correlating to the maximum at 23 u is to low. We assume that due to some electrical discharges the BF_4^- ion is fractured in BF_3 and F^-. The fluorine ion F^- has a mass of 19 u and could be responsible for the maximum visible in the spectrum. Like stated before, this is only based on assumptions and need further validation. We have to improve on the calibration possibilities of the set-up to obtain meaningful information. Nevertheless the data obtained serves as prove of concept for our time of flight set-up and is acceptable as preliminary data.

VI. Conclusion

Multiple internally wetted capillary type emitters fabricated by 3D lithography were presented. Furthermore, the advanced array processing capabilities of the manufacturing method has been displayed, a completely customizable array consisting of more than individual 200 emitters can be manufactured. The emitters exhibit a high printing quality,

high aspect ratio capillaries and well defined features. Individual emitters of an array are almost indistinguishable and are precisely placed. Also presented were simulations for a Bradbury-Nielsen ion gate for time of flight experiments on the manufactured emitters with EMIM-BF_4 as propellant. Based on the simulations the gate was designed in CAD and fabricated afterwards. Preliminary time of flight data obtained from the set-up with the newly integrated Bradbury-Nielsen ion gate was also shown, with a prove of concept for the intended application of characterizing electrospray emitters.

Acknowledgments

The authors gratefully acknowledge funding by the federal state of Hessen and the European Regional Development Fund (ERDF/EFRE 2014 – 2020), Vorhaben: "Innovationslabor: Physik unter harschen Bedingungen" FKZ: FPG991 0002/2019. The time-of-flight setup with improved resolution is being funded by the German Federal Ministry for Economic Affairs and Climate Action under contract (FKZ) 50RS2101.

References

[1] European Space Agency, "ESA's Space Environment Report 2022," *ESA Reports*, 2022. URL `https://www.sdo.esoc.esa.int/environment_report/Space_Environment_Report_latest.pdf`.

[2] Holste, K., Dietz, P., Scharmann, S., Keil, K., Henning, T., Zschätzsch, D., Reitemeyer, M., Nauschütt, B., Kiefer, F., Kunze, F., Zorn, J., Heiliger, C., Joshi, N., Probst, U., Thüringer, R., Volkmar, C., Packan, D., Peterschmitt, S., Brinkmann, K. T., Zaunick, H.-G., Thoma, M. H., Kretschmer, M., Leiter, H. J., Schippers, S., Hannemann, K., and Klar, P. J., "Ion thrusters for electric propulsion: Scientific issues developing a niche technology into a game changer," *Review of Scientific Instruments*, Vol. 91, No. 6, 2020, p. 061101. https://doi.org/10.1063/5.0010134.

[3] Lemmer, K., "Propulsion for CubeSats," *Acta Astronautica*, Vol. 134, 2017, pp. 231–243. https://doi.org/10.1016/j.actaastro.2017.01.048.

[4] Lev, D., Myers, R. M., Lemmer, K. M., Kolbeck, J., Koizumi, H., and Polzin, K., "The technological and commercial expansion of electric propulsion," *Acta Astronautica*, Vol. 159, 2019, pp. 213–227. https://doi.org/https://doi.org/10.1016/j.actaastro.2019.03.058, URL https://www.sciencedirect.com/science/article/pii/S0094576518319672.

[5] Krejci, D., Reissner, A., Seifert, B., Jelem, D., Hörbe, T., Plesescu, F., Friedhoff, P., and Lai, S., "Demonstration of the IFM nano FEEP thruster in low earth orbit," *4S Symposium, Sorrento, Italy*, 2018. URL https://www.researchgate.net/publication/325486881.

[6] Schönherr, T., "Presentaion for the Space Propulsion conference 2022," *8th internatinonal conference on space propulsion, Estoril*, 2022.

[7] Taylor, G. I., "Disintegration of water drops in an electric field," *Proceedings of the Royal Society of London. Series A. Mathematical and Physical Sciences*, Vol. 280, No. 1382, 1964, pp. 383–397. https://doi.org/10.1098/rspa.1964.0151.

[8] Peter, B. S., Dressler, R. A., Chiu, Y.-h., and Fedkiw, T., "Electrospray Propulsion Engineering Toolkit (ESPET)," *Aerospace*, Vol. 7, No. 7, 2020. https://doi.org/10.3390/aerospace7070091.

[9] MacArthur, J., Colicci, V., Barrios, A. T., Kutina, K., and Lozano, P., "Sintered silica ceramics for electrospray propulsion emitters," *8th internatinonal conference on space propulsion, Estoril*, 2022.

[10] Kunze, F. L., Henning, T., and Klar, P. J., "Taking internally wetted capillary electrospray emitters to the sub-ten-micrometer scale with 3D microlithography," *AIP Advances*, Vol. 11, No. 10, 2021, p. 105315. https://doi.org/10.1063/5.0066619, URL https://doi.org/10.1063/5.0066619.

[11] Kunze, F. L., Henning, T., and Klar, P. J., "Validation of pure SU-8 micro 3D printed internally wetted capillary type electrospray mircoemitters for thruster applications," *8th internatinonal conference on space propulsion, Estoril*, 2022.

[12] Gustan-Gutierrez, E., and Gamero-Castaño, M., "Microfabricated Electrospray Thruster Array with High Hydraulic Resistance Channels," *Journal of Propulsion and Power*, Vol. 33, No. 4, 2017, pp. 984–991. https://doi.org/10.2514/1.B36268.

[13] Henning, T., Huhn, K., and Klar, P. J., "Characterisation of electrospray microemitters fabricated by planar and 3D photolithography," *36th International Electric Propulsion Conference (IEPC), Vienna*, 2019. URL http://electricrocket.org/2019/344.pdf.

[14] Huhn, K., Henning, T., Klar, P. J., and Hengsbach, S., "Colloid emitters in photostructurable polymer technology: Fabrication and characterization progress report," *34th International Electric Propulsion Conference, Kobe*, 2015. URL http://electricrocket.org/IEPC/IEPC-2015-120_ISTS-2015-b-120.pdf.

[15] Huhn, K., Piechotka, M., Henning, T., and Klar, P. J., "Investigation of the emission behavior of miniaturized SU-8 based colloid emitters," *33rd International Electric Propulsion Conference, Washington DC*, 2013. URL http://electricrocket.org/IEPC/nl5kwbt2.pdf.

[16] Key, M., Cindro, V., and Lozano, M., "On the radiation tolerance of SU-8, a new material for gaseous microstructure radiation detector fabrication," *Radiation Physics and Chemistry*, Vol. 71, No. 5, 2004, pp. 1003–1007. https://doi.org/10.1016/j.radphyschem.2004.03.002.

[17] Bradbury, N. E., and Nielsen, R. A., "Absolute Values of the Electron Mobility in Hydrogen," *Phys. Rev.*, Vol. 49, 1936, pp. 388–393. https://doi.org/10.1103/PhysRev.49.388, URL https://link.aps.org/doi/10.1103/PhysRev.49.388.